Journal of Power Sources 271 (2014) 8–15

Contents lists available at ScienceDirect

Journal of Power Sources

journal homepage: www.elsevier.com/locate/jpowsour

Facile fabrication of highly porous photoanode at low temperature for all-plastic dye-sensitized solar cells with quasi-solid state electrolyte

Nianqing Fu [a, b, c, 1], Yandong Duan [b, 1], Yanyan Fang [b], Xiaowen Zhou [b], Yanchun Liu [c], Feng Peng [c], Yuan Lin [b, **], Haitao Huang [a, *]

[a] Department of Applied Physics, The Hong Kong Polytechnic University, Hung Hom, Kowloon, Hong Kong, China
[b] Beijing National Laboratory for Molecular Sciences, Key Laboratory of Photochemistry, Institute of Chemistry, Chinese Academy of Sciences, Beijing 100190, China
[c] School of Chemistry and Chemical Engineering, South China University of Technology, Guangzhou 510640, China

HIGHLIGHTS

- Novel inorganic binder contained TiO_2 paste is developed for plastic electrodes.
- The produced films are highly porous and mechanically robust.
- The DSSCs show significant enhancement in charge transport and charge collection.
- A 76% efficiency improvement is observed for the plastic quasi-solid DSSCs.
- The proposed plastic devices are very stable toward shape wrench.

GRAPHICAL ABSTRACT

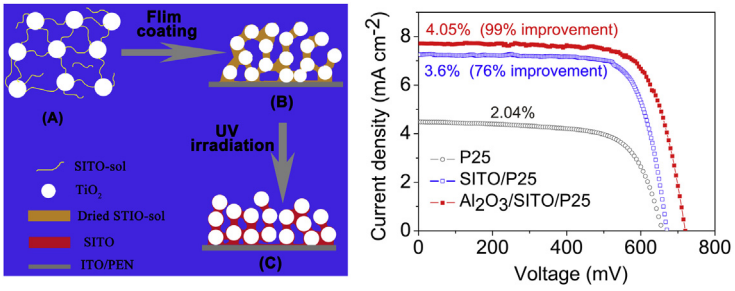

ARTICLE INFO

Article history:
Received 11 June 2014
Received in revised form
28 July 2014
Accepted 29 July 2014
Available online 12 August 2014

Keywords:
Plastic dye-sensitized solar cells
Working electrode
Macroporous
Low temperature
Quasi-solid state electrolyte
Inorganic binder

ABSTRACT

Fabrication of stable plastic solar cells is interesting, but still remains a big challenge. In this study, we develop a facile technique to prepare highly porous TiO_2 hybrid film on plastic substrate for flexible dye-sensitized solar cells (DSSCs) with quasi-solid state electrolyte, employing an inorganic binder contained TiO_2 paste. Compared with a pristine P25 electrode, the obtained photoanode exhibits not only excellent mechanical stability but also improved charge transport property. Moreover, the semiconductor film also shows a highly porous structure with pore volume up to 0.25 $cm^3\ g^{-1}$, allowing unhindered infiltration of viscous quasi-solid state electrolyte. The obtained all-plastic DSSCs with quasi-solid state electrolyte demonstrate a high efficiency up to 3.6%, which is 76% higher than the devices based on pristine P25 electrodes. The cell efficiency can be further increased to 4.05% by depositing an insulating Al_2O_3 layer on the TiO_2 surface to suppress electron recombination. The effects of the inorganic binder on the performance of the hybrid electrodes as well as the DSSCs are investigated by various techniques and measurements.

1. Introduction

As promising and inexpensive alternatives to conventional Si-based solar cells, the third generation of photovoltaics devices, such as dye-sensitized solar cells (DSSCs) and perovskite solar cells, has attracted an increasing amount of attention [1–10]. High power

* Corresponding author. Tel.: +852 2766 5694; fax: +852 2333 7629.
** Corresponding author. Tel.: +86 10 8261 5031; fax: +86 10 8261 7315.
E-mail addresses: linyuan@iccas.ac.cn (Y. Lin), aphhuang@polyu.edu.hk, hthuang2002@yahoo.com (H. Huang).
[1] Nianqing Fu and Yandong Duan contribute equally to this article. The authors declare no competing financial interest.

http://dx.doi.org/10.1016/j.jpowsour.2014.07.181
0378-7753/

conversion efficiency (PCE) over 12% and 15% has been achieved in rigid DSSCs and solid-state perovskite solar cells, respectively [2,9,10]. Recently, many research efforts have been made to replace the rigid glass substrates with plastic ones to fabricate both flexible DSSCs and perovskite solar cells, featuring a roll to roll manufacturing process for flexible, conformable, thin and light-weight photovoltaic devices [6–16].

The photoanode of high performance DSSCs and mesoporous TiO_2-perovskite solar cells should have a porous structure with large surface area, display efficient electrical connectivity, and exhibit tight adhesion to the substrate. Conventional nanocrystalline TiO_2 electrodes are usually prepared by coating the conductive glass with an organic binder contained TiO_2 paste, followed by high-temperature sintering (>450 °C) to remove any organic additives presented in the TiO_2 paste and to guarantee efficient coalescence between the particles [16,17]. Unfortunately, this traditional technique is not feasible when a plastic substrate such as ITO coated PEN (polyethylene naphthalate, ITO/PEN) or PET (polyethylene, ITO/PET) is used to replace the rigid glass one, owing to the thermal instability of the plastic substrates.

Many alternative techniques have been proposed to prepare TiO_2 films at low temperatures [18–27]. Even some of these approaches show great promise, the PCE of those DSSCs prepared by the above techniques were still very low because of the poor TiO_2 film performance. Till now, the mechanical compression method, pioneered by Hagfeldt et al. [6], seems to be the most efficient technique to fabricate plastic semiconductor electrodes for flexible DSSCs with liquid electrolyte [6,28–30].

As one of the three key components of the DSSCs, electrolyte plays a crucial role on not only the PCE, but also the durability of the cell. Till now, except the above mentioned solid-state perovskite solar cells, most of the high efficiency DSSCs employ volatile liquid solutions as the electrolyte [2,3,30]. Unfortunately, the presence of this kind of electrolyte substantially limits the practical application of the DSSCs because of the evaporation and leakage of the electrolyte [4,31]. Replacing the liquid electrolyte with quasi-solid or solid state ones seems to be promising approaches to solving this problem [4,31]. Usually, the quasi-solid and solid state electrolytes have poor permeability and a highly porous photoanode is required for the electrolyte infiltration. Although certain progress has been made to fabricate quasi-solid or solid state DSSCs on rigid glass substrates, little work has been reported on the fabrication of plastic DSSCs with quasi-solid and solid state electrolytes [32–34], owing to the big challenge in the fabrication of highly porous photoanode with high performance at low temperature. Therefore, developing simple techniques for fabricating plastic photoanode with high performance at low temperature for quasi-solid or solid DSSCs is still highly demanded. Moreover, depositing fine grained TiO_2 film on plastic substrate at low temperature for flexible perovskite solar cells is also a hot topic [10].

SnO_2 has demonstrated itself as the alternative host material for DSSCs because of its high electronic conductivity and electron mobility (up to 200 $cm^2\ V^{-1}\ S^{-1}$, which is 100 times higher than that of TiO_2) [35–37]. Herein, we present the fabrication of all-plastic DSSCs with quasi-solid state electrolyte, employing a highly porous plastic photoanode derived from an In/Sb doped SnO_2 sol (SITO-sol) contained TiO_2 paste. Owing to the chemical bridging-effects among the P25 particles by the more conductive In/Sb doped SnO_2 (SITO), the obtained semiconductor film exhibits enhanced mechanical stability as well as improved electron transport property, compared with the pristine P25 electrode. More importantly, the produced electrode demonstrates a high pore volume up to 0.25 $cm^3\ g^{-1}$, facilitating the infiltration of the viscous electrolyte. The quasi-solid DSSCs with plastic hybrid photoanodes under optimum SITO concentration yield a PCE of 3.6%, which is 76% higher than the devices based on pristine P25 electrodes. Depositing an Al_2O_3 insulating layer on TiO_2 surface can further enhance the PCE to 4.05% by suppressing the charge recombination. Additionally, the proposed technique is also promising for the fabrication of plastic perovskite solar cells.

2. Experimental section

2.1. Materials

TiO_2 powders (P25, 20–30 nm) were purchased from Degussa (AG, Germany), The ITO/PEN substrates (15 Ω sq^{-1}, 82% transparency) were obtained from Peccell. The Ru dye, cis-di(thiocyanato)-bis(2,2-bipyridyl-4,4-dicarboxylate) ruthenium(II) (N719), was purchased from Solaronix (Switzerland). All other chemicals were purchased from Alfa Aesar or Acros. All the regents were of analytical purity and used as received.

2.2. Preparation of (Sb, In) doped SnO_2 sol and TiO_2 paste

The preparation of the (Sb, In) doped SnO_2 sol (denoted as SITO-sol) was prepared according to our previous work [38]. In short, 9.6 g tin (II) dichloride dihydrate was dissolved in 50 mL anhydrous ethanol, and 3 mL distilled water was added subsequently. This mixture was refluxed at 80 °C for 7 h. Then, another 10 mL C_2H_5OH solution containing 0.66 g antimony chloride and 0.38 g indium chloride was added dropwise into the tin chloride mixture and refluxed at 80 °C for 3 h. The resulting mixture was aged for one week at room temperature to yield a light yellow sol.

TiO_2 powder (P25, Degussa) was pre-sintered at 450 °C for 30 min before use [17]. 0.6 g P25 powder was dispersed in a mixture of anhydrous ethanol and *n*-butanol (v/v = 1:1) by 12 h magnetic stirring, followed by 1 h ultrasonic dispersion to form a uniform TiO_2 colloid. For the SITO-sol incorporated TiO_2 paste (SITO-sol/P25), certain volume of SITO-sol (0, 50, 100, 200, 300, and 400 μL) was added into the as-prepared pristine TiO_2 colloid, followed by 1 h of gentle stirring before coating onto the substrate. The weight percentage (wt%) of the total metal oxide (TiO_2 + doped SnO_2) in all paste was kept at 16 wt% by varying the amount of dispersant.

2.3. Fabrication of photoanode and assembly of plastic DSSCs

Before film coating, a very thin TiO_2 compact layer (about 10 nm) was deposited on the well cleaned ITO/PEN substrates according to our previous work [15]. SITO-sol/P25 pastes with varying amounts of SITO-sol were spread on the substrates by a doctor-blade technique. The film thickness of all electrodes was controlled to be 10 ± 0.2 μm. After drying in air, the films were exposed to UV irradiation (300 W) for 30 min. The as-prepared SITO contained electrodes were immersed in 100 °C distilled water for 30 min to remove any residues introduced by the SITO-sol. The electrodes derived from pristine P25 colloid and the SITO-sol/P25 paste are denoted as P25 and SITO/P25, respectively. The coating of a thin Al_2O_3 layer was carried out by dipping the as-prepared films into a hot 2-propanol-based solution of aluminum sec-butoxide (20 mM, 50 °C) for 3 min, followed by air drying (80% humidity) and immersing in 100 °C distilled water for 30 min. All electrodes were dried at 100 °C in an oven for 1 h before sensitized in 0.5 mM N719 dye/ethanol solution overnight.

Plastic counter electrodes (CEs) were prepared through a photoplatinization technique [15]. In short, the ITO/PEN substrate was modified by ~25 nm TiO_2 layer produced by spin-coating and hydrolysis of tetra-n-butyl titanate. The modified substrates were immerged in 0.13 mM H_2PtCl_6/2-propanol solution and exposed to

UV irradiation for about 1 h to deposit Pt on the TiO_2 surface. Plastic DSSCs were assembled using the as-prepared photoanodes and the plastic CEs, employing a quasi-solid state electrolyte which was prepared according to our previous work [31].

2.4. Measurements and characterizations of the TiO_2 electrodes and DSSCs

The surface morphology of the electrodes was investigated by scanning electron microscopy (SEM/EDX, Hitachi S-4800, 15 kV) and high resolution transmission electron microscopy (TEM, JEM 2011, Japan; 200 kV). The mechanical adhesion strength of the TiO_2 photoelectrode was measured by scratching the TiO_2 film with a standard pencil, according to the ISO/DIS 15184 method [30]. The adhesion strength of the film was measured by the bending test similar to the reported work [39]. The surface area and pore distribution were evaluated using a Quantachrome NOVA 2000e analyzer. The detection range of the pore diameter is between 1.7 and 300 nm. The Brunauer–Emmett–Teller (BET) and Barrent–Joyner–Halenda (BJH) methods were used to estimate the specific surface area (SSA) and the pore size distribution, respectively. The photocurrent–voltage curves were recorded using a computer-programmed Keithley 2611 SourceMeter under simulated sunlight illumination (AM 1.5, 100 mW cm^{-2}) supplied by a solar simulator (Oriel, 91160-1000 91192, Perccell Technologies). The intensity-modulated photocurrent spectroscopy (IMPS) and intensity-modulated photovoltage spectroscopy (IMVS) measurements were performed on the same sandwiched cells, using a green light emitting diode (LED, peak wavelength 520 nm) driven by a Solartron 1255B frequency-response analyzer. The LED provides both dc and ac components of the illumination. The light intensities were modulated (±8%) by modulating the voltage applied to the LED.

3. Results and discussion

3.1. Formation of hybrid electrodes and their mechanical properties

Scheme 1 represents the technique for preparation of the plastic electrode at low temperature. When the SITO-sol (Fig. S1 in Supplementary materials) is added into the liquid TiO_2 colloid, the Sn–OH active head groups of the HO–$(Sn–O–Sn)_n$–OH chains react with the hydroxyl groups on the TiO_2 particle surface to form cross-linked network. The SITO-sol in the paste acts both as an inorganic binder and a kind of surfactant. After the SITO-sol/P25 paste was spread onto the substrate and dried in the air, the SITO-sol shrinks gradually at the grain boundaries by capillary force upon solvent evaporation. During the subsequent UV-irradiation, the dried SITO-sol converted into SITO crystals with a tetragonal rutile structure [38], which bridged the individual TiO_2 particles and also formed firm connections between the film and the TiO_2 modified ITO/PEN substrate.

The mechanical rigidity is one of the most important properties of the electrode, especially for plastic devices with quasi-solid state electrolyte since the semiconductor films in contact with the viscous gel-state electrolyte is more liable to be damaged during the shape wrench of the devices. Hardness and bending tests were employed to evaluate the mechanical stability of the films. The effects of the SITO contents on the hardness of the hybrid film are illustrated in Fig. 1. The pristine P25 film is easily destroyed by a 6B pencil, while the incorporation of the SITO continuously increases the hardness of the films. The hybrid film with 4 wt% SITO demonstrates a hardness up to HB grade, and this value further increases to 3H with 10 wt% SITO incorporation. The increased film hardness can be attributed to the formation of rigid bridges between TiO_2 particles by SITO crystals, which will be shown later. The excellent adhesion of the SITO/P25 film to the substrate was confirmed by bending test. The inset in Fig. 1 demonstrates that no changes can be observed for the SITO/P25 (4 wt%) hybrid electrode after fifty cycles of concave and convex bending. In contrast, the P25 film is desquamated by just one cycle of bending.

3.2. Influence of SITO on the surface morphology of the TiO_2 electrodes

The cross-sectional SEM images of the electrodes with various amounts of SITO (ca. 0, 4, 6, and 10 wt%, respectively) shown in Fig. 2 demonstrate that both the pore number and pore size can be altered by the SITO amount. Appropriate amount of SITO (ca. 4 wt%, Fig. 2b) in TiO_2 increases the number of pores and enlarge the pore size as well. However, excessive SITO (ca. 10 wt%) obstructs the pores, decreasing the pore size and pore number (Fig. 2d). The pore structure of the film is crucial to the infiltration of the viscous electrolyte and affects the cell performance subsequently. The TEM images in Fig. 3a and b reveal that continuous network morphology still remained even though the SITO/P25 film had been subjected to two hours of strong ultrasonication. By contrast, the P25 film disintegrated into small aggregates after the similar treatment. High

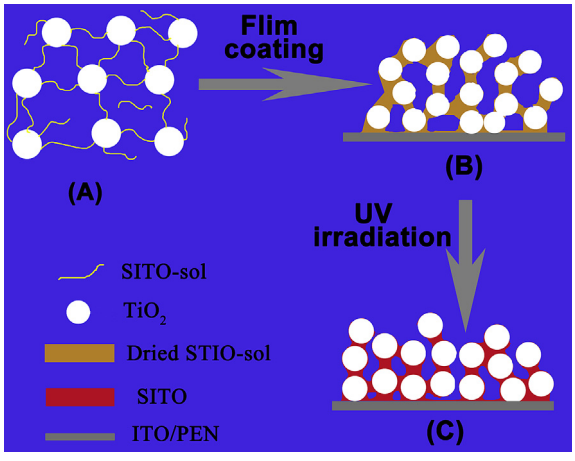

Scheme 1. Schematic representation of the preparation of hybrid TiO_2 electrodes, employing a Sb/In doped SnO_2 sol contained TiO_2 paste.

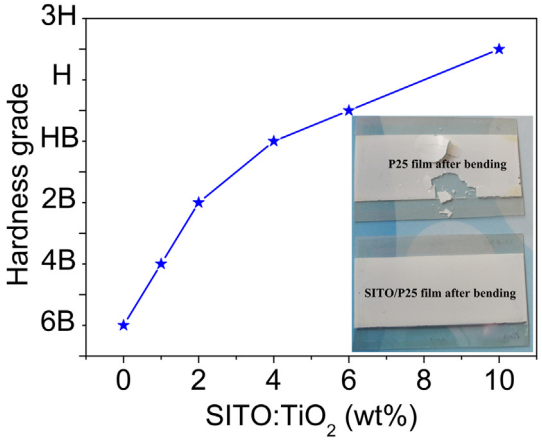

Fig. 1. The hardness of the semiconductor films with various SITO incorporation, tested according to the ISO/DIS 15184 method. The insets are digital images of P25 (top) and SITO/P25 (bottom) electrodes after one cycle and fifty cycles of bending test, respectively.

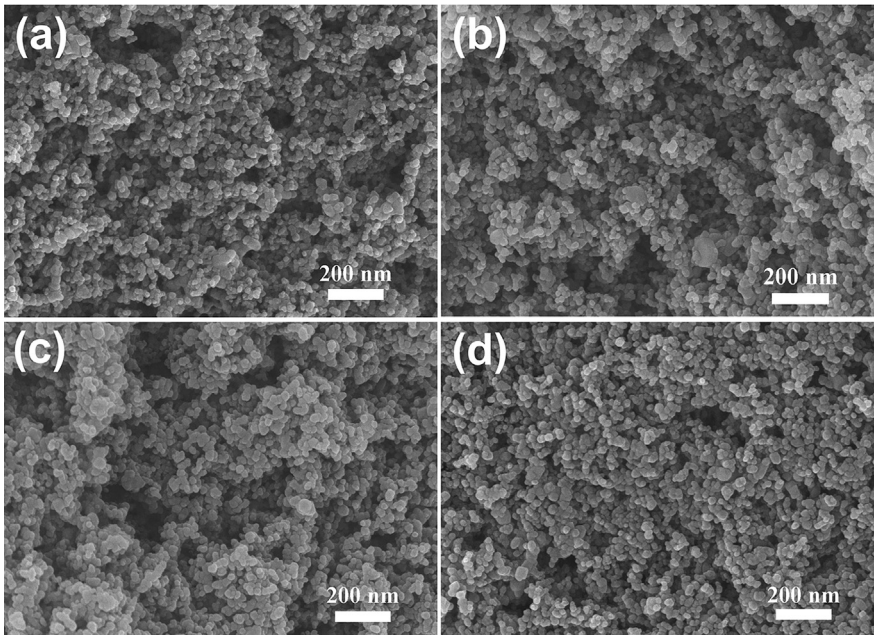

Fig. 2. Cross-sectional high-resolution SEM micrographs of SITO/P25 electrodes with (a) 0 wt%, (b) 4 wt%, (c) 6 wt%, and (d) 10 wt% SITO, respectively.

magnification TEM images (Fig. 3c and d) confirm that the TiO_2 particles in SITO/P25 hybrids are bridged by SITO while the stacking of the TiO_2 particles in the pristine P25 film relies only on their physical contact. The formation of SITO/P25 network not only promises the semiconductor film excellent mechanical stability but also provides a continuous pathway for the efficient and fast charge transport in the hybrid films.

The electrodes with various SITO were examined by nitrogen adsorption–desorption measurements and analyzed by means of BJH and BET to further study the effects of the SITO on the morphological changes of the films. The measurements were carried out on the film fragments which were carefully peeled off from the ITO-free PEN substrate. The pore-size distribution, pore volume and average pore size obtained via the BJH model derived from the desorption branch are present in Fig. 4 and Table 1, respectively. The pore-size distribution curves demonstrate that small pores with several nanometer in diameter are easily crammed by even a small amount of SITO, while a proper amount of SITO (ca. 2, and 4 wt%) can enlarge the size of bigger pores, with a diameter in tens to hundreds of nanometer, and increase the pore volume as well. In contrast, excess SITO (10 wt%) decreases both the pore size and pore volume. This observation is in accordance with the results deduced from SEM observations. The average pore diameters of the films with 0, 2, 4, 6, and 10 wt% SITO incorporation are 17.08, 21.18, 25.83, 15.78, and 9.36 nm, respectively, with pore volumes (for pores with a diameter in the range of 1.7–300 nm) of 0.22, 0.23,

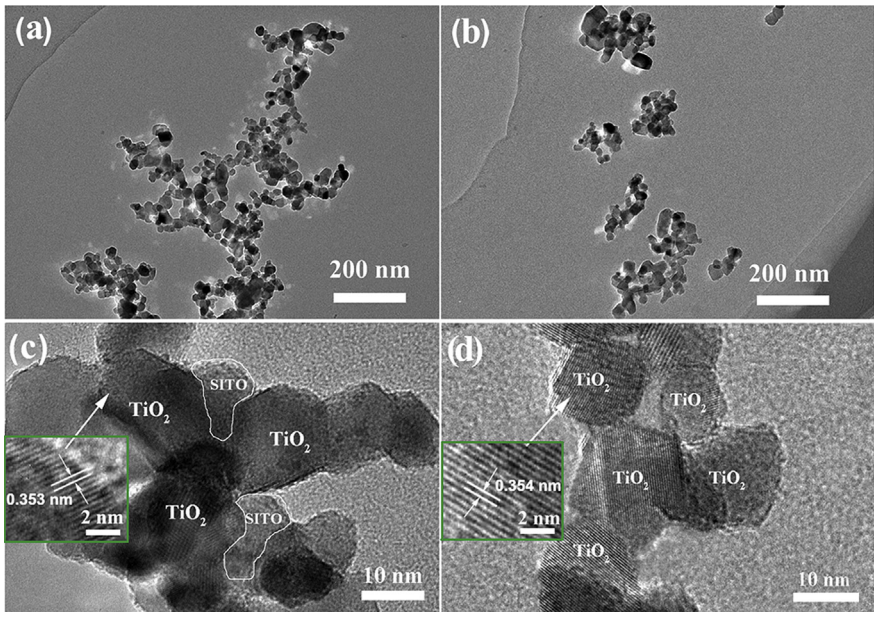

Fig. 3. TEM images of sample from (a, c) SITO/P25 (4 wt% SITO) and (b, d) P25 film. The samples for TEM tests were prepared by 2 h' strong ultrasonication of the films.

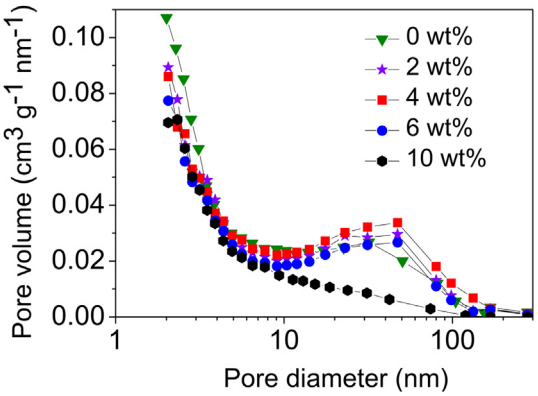

Fig. 4. Pore-size distribution of the film with various amounts of SITO (ca. 0, 2, 4, 6, 10 wt%).

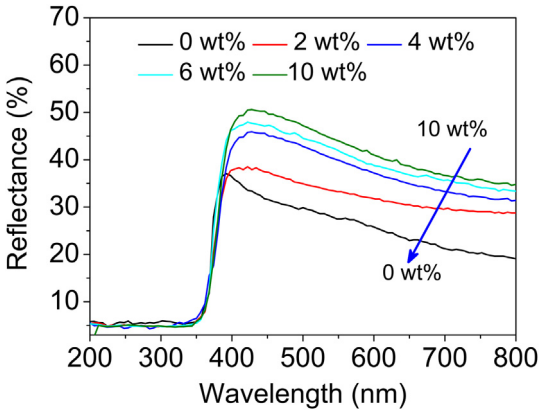

Fig. 5. Reflectance spectra of P25 and STIO/P25 electrodes with different amounts of SITO incorporation.

0.25, 0.21, and 0.13 $cm^3\ g^{-1}$, respectively. The BET results listed in Table 1 reveal that the specific surface area (SSA) decreases from 57.7 to 42.4 $m^2\ g^{-1}$ with the amount of SITO increased from 0 to 10 wt%, since the SITO covers the joints of TiO_2 particles or even fills into the pores (Figs. 2–4), decreasing the SSA consequently.

The light scattering property and dye-loadings of the films were tested to further evaluate the effects of SITO on the electrode performance. As shown in Table 1, the addition of SITO lowers the dye-loading of the films because of (1) the reduced SSA and (2) the relative poorer dye-absorption capacity of the SnO_2, as compared to TiO_2 [40]. The decrease of dye-loading will, in principle, decline the light harvesting of the photoanode employing SITO/P25. The light scattering property of the films shown in Fig. 5 reveals that the incorporation of the SITO leads to an appreciable enhancement in diffuse light scattering, since the SITO connects the TiO_2 particles to form aggregates with mixed sizes, leading to light-scattering and light-confinement effects [21,29]. The light scattering and confinement effects can extend the optical path length of the film, which enhances the probability of photons being captured by the dye molecules and finally improves the short-circuit current (J_{sc}) of the device.

3.3. The photovoltaic performance of DSSCs

The photovoltaic characteristics of the plastic quasi-solid DSSCs as a function of the SITO contents are shown in Fig. 6. The open-circuit voltage (V_{oc}) of the devices first increases slightly and then decreases with further increasing of SITO content. The formation of continuous pathway and tight adhesion of the SITO/P25 film to the substrate will facilitate fast charge transport and transfer and suppresses charge recombination consequently, leading to higher V_{oc} at low SITO content. However, SITO has a deeper conduction band than TiO_2, which should, in principle, lower the Fermi level of the film and decreases the V_{oc} [35,36]. Additionally, too much SnO_2 with deeper conduction band will form electronic traps which lead to faster interfacial charge recombination and thus further lower the V_{oc} [35]. The short-circuit current density (J_{sc}) of the DSSCs increases at low SITO concentration, reaching a peak value at 4 wt% SITO incorporation, and then begins to decrease with further increasing of SITO. The increased J_{sc} at low SITO concentration (no more than 4 wt%) results from the positive effects of the SITO incorporation, such as enhanced electron transport and transfer, improved electron collection efficiency (will be discussed later) and enhanced light-scattering. In contrast, in the case of high SITO concentrations, the decreased dye-loading, increased electron recombination and poor electrolyte infiltration will decline the J_{sc}. The PCE of the DSSCs exhibits a similar trend to the J_{sc} values, attaining the maximum value with 4 wt% SITO.

The *J–V* characteristic curves and the corresponding photovoltaic parameters of the quasi-solid plastic DSSCs employing pristine P25 and SITO/P25 hybrid (4 wt% SITO) photoanodes are displayed in Fig. 7 and Table 2. The J_{sc}, V_{oc}, FF and PCE of the P25 cells are 4.66 mA cm^{-2}, 660 mV, 0.674 and 2.04%, respectively. The J_{sc} and FF of the SITO/P25 cells are 7.25 mA cm^{-2} and 0.741, respectively,

Table 1
The BET surface area, pore volume, pore size, and dye-loadings of the P25 and SITO/P25 electrodes with 2, 4, 6, and 10 wt% SITO.[a]

SITO content [%]	Surface area[b] [$m^2\ g^{-1}$]	Pore volume[c] [$cm^3\ g^{-1}$]	Pore size[d] [nm]	Dye-loading [10^{-7} mol cm^{-2}]
0	57.7	0.22	17.08	0.67
2	56.4	0.23	21.18	0.65
4	53.1	0.25	25.83	0.62
6	50.6	0.21	15.78	0.58
10	42.4	0.13	9.36	0.47

[a] The data in the table are the mean values of three samples.
[b] BET surface area.
[c] BJH desorption cumulative volume of pores between 1.7000 nm and 300.0000 nm diameter.
[d] BJH desorption average pore diameter (4 V/A).

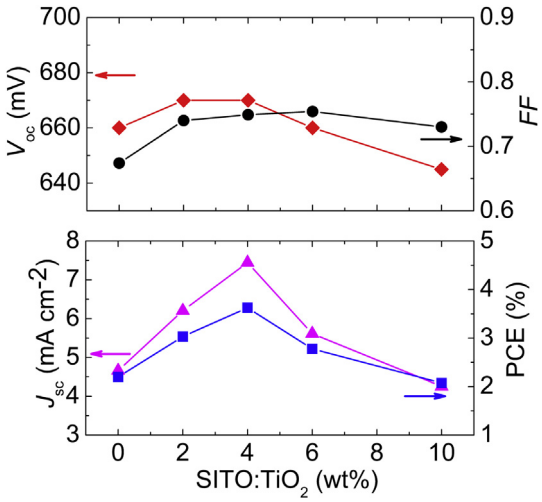

Fig. 6. Open-circuit voltage (V_{oc}, ◆), fill factor (FF, ●), short-circuit current density (J_{sc}, ▲) and power conversion efficiency (PCE, ■) of the DSSCs as a function of SITO content in the TiO_2 paste, respectively.

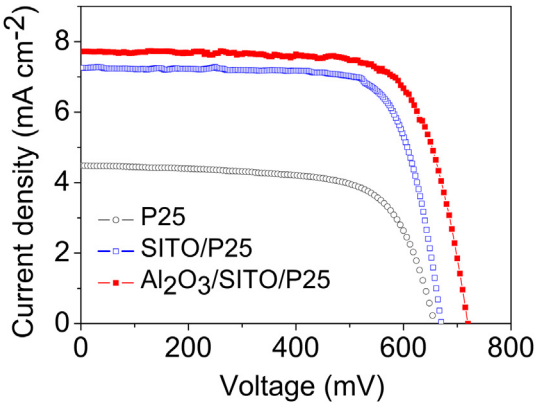

Fig. 7. Current–voltage curves of DSSCs employing different photoanodes. P25, SITO/P25, Al_2O_3/SITO/P25, and P25-C represent the pristine P25 electrode, 4 wt% SITO incorporated SITO/P25 hybrid electrode, Al_2O_3 coated SITO/P25 hybrid electrode, and P25 electrode prepared by 100 MPa mechanical compression, respectively.

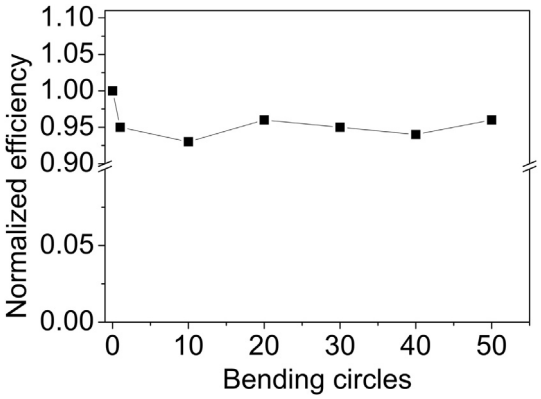

Fig. 8. The normalized efficiency variation of the SITO/P25 cells (4 wt% SITO) with the circles of bending test.

which are significantly higher than those of the P25 ones. As a result, the SITO/P25 devices demonstrate a PCE up to 3.6%, improved by 76%, as compared with the P25 cell. The enhanced light-scattering property (as shown in Fig. 5), faster electron transport and improved charge collection efficiency (which will be discussed in Section 3.4) account for the improved J_{sc}. The decreased series resistance of the SITO/P25 electrode results in a higher FF. Noticeably, though the carefully handled pristine P25 cells yield an efficiency of 2.04%, the bending tests reveal that they are not practically useful as flexible devices because the electrolyte infiltrated film are easily detached off from the substrate during the shape wrench, owing to the poor adhesion of the semiconductor film to the substrate. In contrast, almost no efficiency deterioration can be observed when the SITO/P25 (4 wt% SITO) cells were subjected to fifty circles of concave and convex bending (shown in Fig. 8), indicating that the plastic DSSCs produced by the proposed technique have the potential for practical application as flexible devices. For comparison, the proposed TiO_2 pastes were also used to fabricate DSSCs on rigid FTO glass at different temperatures. The IV results of those cells are shown in Fig. S2 and Table S1. The PCE of the SITO/P25 (4 wt% SITO) and P25 cells fabricated on glass substrate at low temperature is 3.91% and 2.32%, respectively. The 68% enhancement in efficiency is similar to that of the cells fabricated on plastic substrate. The high temperature (450 °C) sintering of the photoanode on glass substrate results in a PCE of 4.29% for the SITO/P25 cell, 22% higher than that of the P25 one (PCE = 3.53%). It is also noted that the high temperature sintering improves the PCE of SITO/P25 cell by 10% (from 3.91% to 4.29%), while this value is 52% for the P25 cell (from 2.32% to 3.53%). This is because the high temperature annealing can effectively enhance the physical and electrical connections among TiO_2 nanoparticles, while the effect of SITO on the enhancement of the physical and electrical connections becomes less significant.

It was reported that the recombination rate increases by 2–3 orders of magnitude when a high mobility material, such as SnO_2, is in direct contact with the sensitizer and/or the electrolyte [35–37]. In this case, further improvement in the DSSC performance can be anticipated by depositing a thin insulating layer to suppress the electron recombination due to the SITO. As shown in Fig. 7 and Table 2, the J_{sc}, V_{oc}, and FF of the Al_2O_3 coated SITO/P25 cell (Al_2O_3/SITO/P25) are 7.71 mA cm^{-2}, 715 mV, and 0.732, respectively, leading to a PCE improvement from 3.6% to 4.05%. Compared with the SITO/P25 cell, the PCE improvement of the Al_2O_3/SITO/P25 cell results from the enhanced V_{oc} and J_{sc}. The improvement of V_{oc} is attributed to the reduced electron recombination and shift of the Fermi level. On one hand, the charge-blocking effect of the Al_2O_3 insulating layer prohibits the electron recombination from the SITO/P25 to the redox electrolyte and increases the V_{oc} in return. On the other hand, the insulating Al_2O_3 layer will shift the Fermi level of the Al_2O_3/SITO/P25 film and enlarges the difference between the Fermi level and the redox potential of the I_3^-/I^-, leading to increased V_{oc}. The increase in J_{sc} is ascribed to (1) the improved dye adsorption (from 0.62×10^{-7} to 0.66×10^{-7} mol cm^{-2}) due to the more favorable dye adsorption on the surface of Al_2O_3 than TiO_2 [40] and (2) the suppressed electron recombination.

Table 2
Photovoltaic characteristics of DSSCs with different photoanodes, measured under AM 1.5 simulated illumination of 100 mW cm^{-2}.[a]

Photoanodes	J_{sc} [mA cm^{-2}]	V_{oc} [mV]	FF	PCE [%]
P25	4.66	660	0.674	2.04
SITO/P25	7.25	670	0.741	3.60
Al_2O_3/SITO/P25	7.71	715	0.732	4.05

[a] The data in the table are the mean values of five samples.

3.4. Electrochemical and electrical properties of the photoanodes and DSSCs

IMPS and IMVS, which are commonly employed in the characterization of DSSCs [17,41], were used to investigate the charge transport and recombination process in the DSSCs with different photoanodes. The IMPS and IMVS plots display a semicircle in the complex plane. The electron recombination and transport behavior can be evaluated by the electron lifetime (τ_n) and the electron transport time (τ_d), respectively. τ_n and τ_d can be estimated from the $\tau = (2\pi f_{min})^{-1}$, where f_{min} is the frequency corresponding to the bottom of the semicircle at the IMVS and IMPS plots respectively. Fig. 9 shows the IMPS and IMVS spectrum of pristine P25, SITO/P25, and Al_2O_3/SITO/P25 based plastic DSSCs. The electron transport time (τ_d) of the SITO/P25 cell is 22.4 ms, much shorter than that of the P25 cell (46 ms). As demonstrated in Fig. 3, the existence of the more conductive SITO among TiO_2 particles forms a continuous network, which facilitates the efficient and fast charge transport in the semiconductor hybrid film. The I–V curves of the P25 and the SITO/P25 films are shown in Fig. S3 (Supplementary materials). The current response at 10 V for the SITO/P25 film is 12.2 μA, almost 30-fold higher than that of the P25 film (0.43 μA), implying that the formation of continuous SITO/P25 network significantly decreases the film resistance. The significant decrease of charge transport resistance in the SITO/P25 electrode was also revealed by the

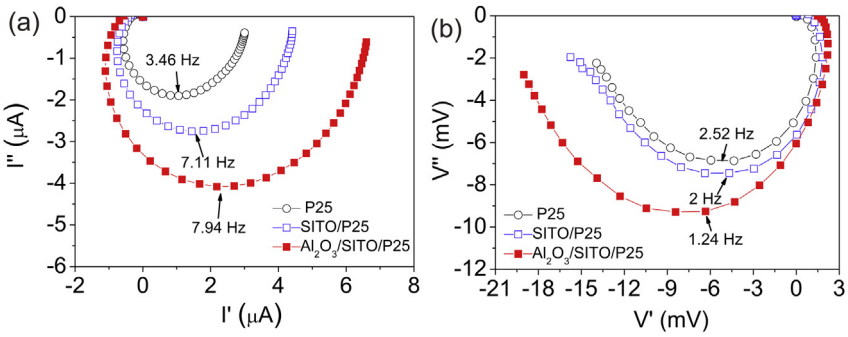

Fig. 9. (a) IMPS and (b) IMVS complex plane plots of plastic DSSCs based on P25, SITO/P25, Al_2O_3/SITO/P25, and P25-C electrodes.

electrochemical impedance spectroscopy (EIS) measurement in real DSSC system, as demonstrated in our previous work [38]. The decreased charge transport resistance results in shorter τ_d. The electron lifetime (τ_n) of the SITO/P25 is 79.6 ms, higher than that of P25 (63.2 ms). The faster charge transport in the SITO/P25 film will decrease the possibility of the electrons to be recombined and leads to longer τ_n. The coating of the insulating Al_2O_3 layer on SITO/TiO_2 surface can suppress the electron recombination remarkably, hence further increasing the τ_n from 79.6 to 126.4 ms. The charge collection efficiency η_{cc} can be determined by the equation of $\eta_{cc} = 1 - \tau_d/\tau_n$ [40]. The η_{cc} increases from 49.8% for P25 to 71.9% for SITO/P25 (4 wt%) based cells. It further improves to 84.1% when an insulating Al_2O_3 layer was deposited on the SITO/P25 surface to suppress electron recombination. The high η_{cc} is a crucial factor for the SITO/P25 DSSCs to yield a high efficiency.

4. Conclusion

In this study, we have demonstrated a simple and effective method for the fabrication of porous and robust SITO/TiO_2 hybrid electrode on ITO/PEN substrate at low temperature for plastic DSSC applications. In addition to flexibility and mechanical stability, the produced films exhibit other meritorious characteristics, such as, excellent porosity, improved light-scattering, enhanced electron transport and decreased electron recombination. Owing to the complete infiltration of the quasi-solid state electrolyte and high charge collection efficiency, the obtained all-plastic quasi-solid DSSCs yield a PCE up to 3.6%, 76% higher than that of the pristine P25 based device. The SITO/P25 also demonstrates outstanding stability toward shape wrench. The deposition of an insulating Al_2O_3 layer on the SITO/TiO_2 surface further improves the efficiency of the SITO/P25 device to 4.05%, by suppressing the electron recombination. The encouraging performance of the DSSCs with gel electrolytes suggests that the method developed in this work is promising for the fabrication of plastic electrodes for solid state plastic-DSSCs or flexible perovskite solar cells.

Acknowledgments

This work was financially supported by National Research Fund for Fundamental Key Project (2012CB932903), Foundation of Chinese Academy of Sciences (KGCX2-YW-386-2). This work was also partially supported by grants received from the Research Grants Council of the Hong Kong Special Administrative Region (PolyU5159/13E and PolyU5163/12E).

Appendix A. Supplementary data

Supplementary data related to this article can be found at http://dx.doi.org/10.1016/j.jpowsour.2014.07.181.

References

[1] B. O'Regan, M. Grätzel, Nature 353 (1991) 737–740.
[2] A. Yella, H.W. Lee, H.N. Tsao, C. Yi, A.K. Chandiran, M.K. Nazeeruddin, E.W.G. Diau, C.Y. Yeh, S.M. Zakeeruddin, M. Grätzel, Science 334 (2011) 629–634.
[3] C.T. Yip, H.T. Huang, L.M. Zhou, K.Y. Xie, Y. Wang, T. Feng, J. Li, W.Y. Tam, Adv. Mater. 23 (2011) 5624–5628.
[4] I. Chung, B. Lee, J.Q. He, R.P.H. Chang, M.G. Kanatzidis, Nature 485 (2012) 486–490.
[5] M. Guo, K.Y. Xie, J. Lin, Z. Yong, C.T. Yip, L.M. Zhou, Y. Wang, H.T. Huang, Energy Environ. Sci. 5 (2012) 9881–9888.
[6] H. Lindström, A. Holmberg, E. Magnusson, S.E. Lindquist, L. Malmqvist, A. Hagfeldt, Nano Lett. 1 (2001) 97–100.
[7] M. Dürr, A. Schmid, M. Obermaier, S. Rosselli, A. Yasuda, G. Nelles, Nat. Mater. 4 (2005) 607–611.
[8] S. So, K. Lee, P. Schmuki, J. Am. Chem. Soc. 134 (2012) 11316–11318.
[9] J. Burschka, N. Pellet, S.J. Moon, R. Humphry-Baker, P. Gao, M.K. Nazeeruddin, M. Grätzel, Nature 499 (2013) 316–319.
[10] D. Liu, T.L. Kelly, Nat. Phot. 8 (2014) 133–138.
[11] J.H. Wu, Y.M. Xiao, Q.W. Tang, G.T. Yue, J.M. Lin, M.L. Huang, Y.F. Huang, L.Q. Fan, Z. Lan, S. Yin, T. Sato, Adv. Mater. 24 (2012) 1884–1888.
[12] F.Z. Huang, D.H. Chen, L. Cao, R.A. Caruso, Y.B. Cheng, Energy Environ. Sci. 4 (2011) 2803–2806.
[13] W. Wang, Q. Zhao, H. Li, H.W. Wu, D.C. Zou, D.P. Yu, Adv. Funct. Mater. 22 (2012) 2775–2782.
[14] Y.L. Li, D.K. Lee, J.Y. Kim, B.S. Kim, N.G. Park, K. Kim, J.H. Shine, I.S. Choi, M.J. Ko, Energy Environ. Sci. 5 (2012) 8950–8957.
[15] N.Q. Fu, Y.Y. Fan, Y.D. Duan, X.W. Zhou, X.R. Xiao, Y. Lin, ACS Nano 6 (2012) 9596–9605.
[16] V. Zardetto, F.D. Giacomo, D. Garcia-Alonso, W. Keuning, M. Creatore, C. Mazzuca, A. Reale, A.D. Carlo, T.M. Brown, Adv. Energy Mater. 3 (2013) 1292–1298.
[17] D.S. Zhang, T. Yoshida, T. Oekermann, K. Furuta, H. Minoura, Adv. Funct. Mater. 16 (2006) 1228–1234.
[18] F. Pichot, J.R. Pitts, B. Gregg, Langmuir 16 (2000) 5626–5630.
[19] X. Li, H. Lin, J.B. Li, X.X. Li, B. Cui, L.Z. Zhang, J. Phys. Chem. C 112 (2008) 13744–13753.
[20] K. Fan, T.Y. Peng, J.N. Chen, K. Dai, J. Power Sources 196 (2011) 2939–2944.
[21] H.W. Chen, C.P. Liang, H.S. Huang, J.G. Chen, R. Vittal, C.Y. Lin, K.C.W. Wu, K.C. Ho, Chem. Commun. 47 (2011) 8346–8348.
[22] H.W. Chen, Y.T. Liao, J.G. Chen, K.C.W. Wu, K.C. Ho, J. Mater. Chem. 21 (2011) 17511–17518.
[23] S. Uchida, M. Tomiha, H. Takizawa, M. Kawaraya, J. Photochem. Photobiol. A 164 (2004) 93–96.
[24] S.I. Cha, B.K. Koo, K.H. Hwang, S.H. Seo, D.Y. Lee, J. Mater. Chem. 21 (2011) 6300–6304.
[25] H. Lee, D. Hwang, S.M. Jo, D. Kim, Y. Seo, D.Y. Kim, ACS Appl. Mater. Interfaces 4 (2012) 3308–3315.
[26] N.G. Park, K.M. Kim, M.G. Kang, K.S. Ryu, S.H. Chang, Y.J. Shin, Adv. Mater. 17 (2005) 2349–2353.
[27] H.C. Weerasinghe, G.V. Franks, J.D. Plessis, G.P. Simon, Y.B. Cheng, J. Mater. Chem. 20 (2010) 9954–9961.
[28] W.H. Chiu, K.M. Lee, W.F. Hsieh, J. Power Sources 196 (2011) 3683–3687.
[29] T. Yamaguchi, N. Tobe, D. Matsumoto, H. Arakawa, Chem. Commun. 45 (2007) 4767–4769.
[30] T. Yamaguchi, N. Tobe, D. Matsumoto, T. Nagai, H. Arakawa, Sol. Energy Mater. Sol. Cells 94 (2010) 812–816.
[31] Y.Y. Fang, J.B. Zhang, X.W. Zhou, Y. Lin, S.B. Fang, Electrochim. Acta 68 (2012) 235–239.
[32] L.C. Chen, J.M. Ting, Y.L. Lee, M.H. Hon, J. Mater. Chem. 22 (2012) 5596–5601.
[33] S.A. Haque, E. Palomares, H.M. Upadhyaya, L. Otley, R.J. Potter, A.B. Holmes, J.R. Durrant, Chem. Commun. (2003) 3008–3009.

[34] Z.S. Xue, C.Y. Jiang, L. Wang, W. Liu, B. Liu, J. Phys. Chem. C (2013), http://dx.doi.org/10.1021/jp408663d.
[35] C.T. Gao, X.D. Li, B.G. Lu, L.L. Chen, Y.Q. Wang, F. Teng, J.T. Wang, Z.X. Zhang, X.J. Pan, E.Q. Xie, Nanoscale 4 (2012) 3475–3481.
[36] N. Tétreault, É. Arsenault, L.P. Heiniger, N. Soheilnia, J. Brillet, T. Moehl, S. Zakeeruddin, G.A. Ozin, M. Grätzel, Nano Lett. 11 (2011) 4579–4584.
[37] A.N.M. Green, E. Palomares, S.A. Haque, J.M. Kroon, J.R. Durrant, J. Phys. Chem. B 109 (2005) 12525–12533.
[38] N.Q. Fu, Y.D. Duan, Y.Y. Fang, X.W. Zhou, X.R. Xiao, Y. Lin, Electrochem. Commun. 34 (2013) 254–257.
[39] X.L. He, M. Liu, G.J. Yang, H.L. Yao, S.Q. Fan, J. Li, J. Power Sources 226 (2013) 173–178.
[40] A. Kay, M. Grätzel, Chem. Mater. 14 (2002) 2930–2935.
[41] Y.D. Duan, N.Q. Fu, Q.P. Liu, Y.Y. Fang, X.W. Zhou, J.B. Zhang, Y. Lin, J. Phys. Chem. C 116 (2012) 8888–8893.